Figure S1. The spatial distribution of raw DMS observational data in GSSD database.
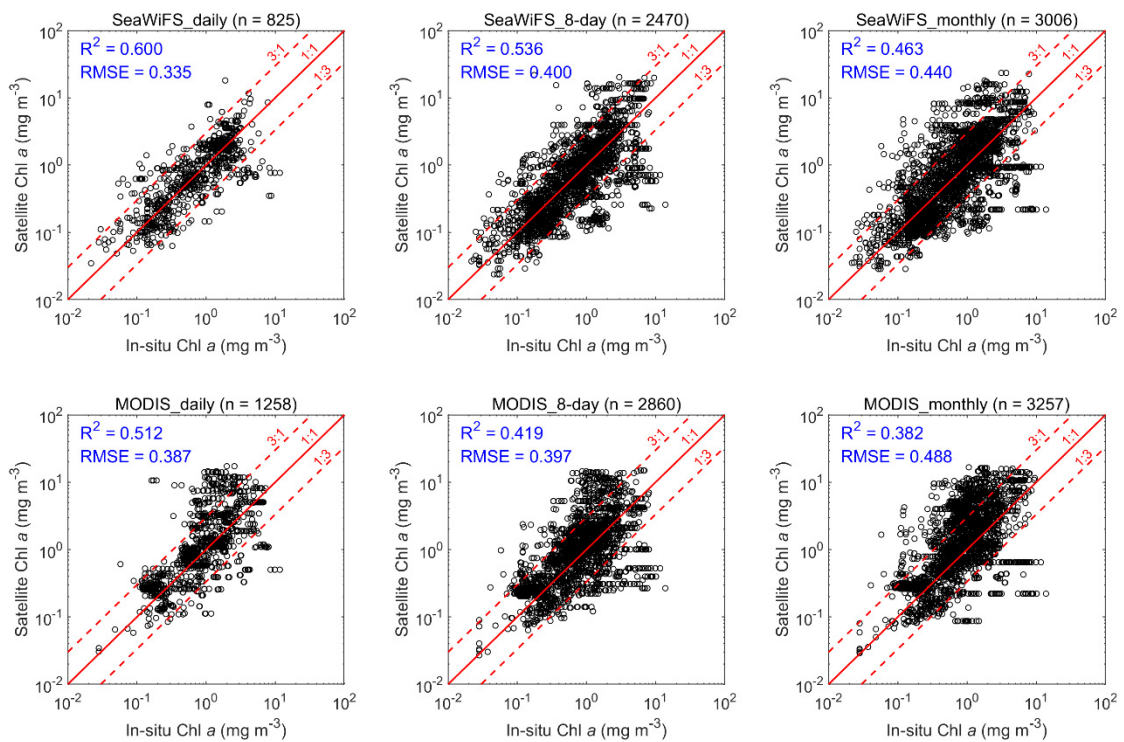
Figure S2. The comparison between the in-situ Chl *a* from GSSD database and the Chl *a* retrieved from different satellites. n is the number of samples. R^2 and RMSE correspond to $\log_{10}$ space data.
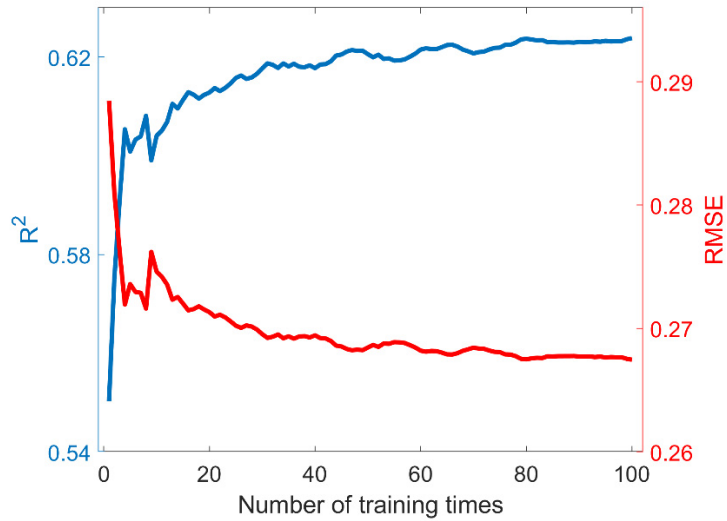
Figure S3. The changes of R^2 and RMSE between the averaged simulation results and observed DMS concentrations along with the increase of training times.
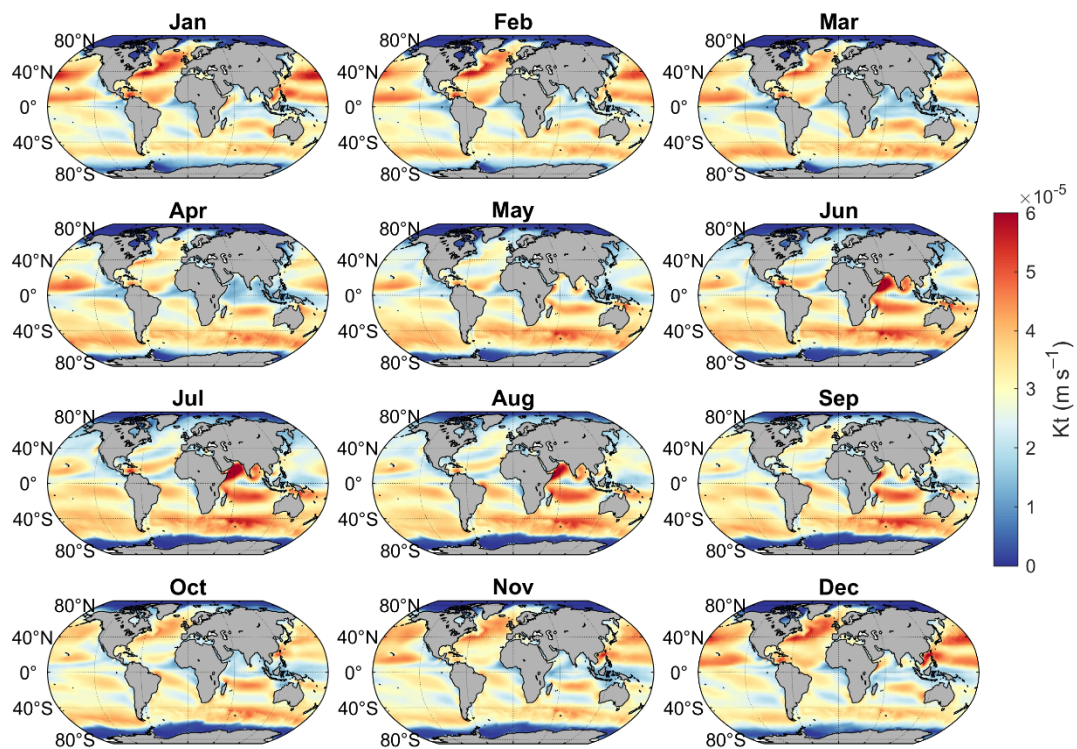
Figure S4. Monthly climatology of the total transfer velocity (Kt) of DMS during 1998 to 2017.
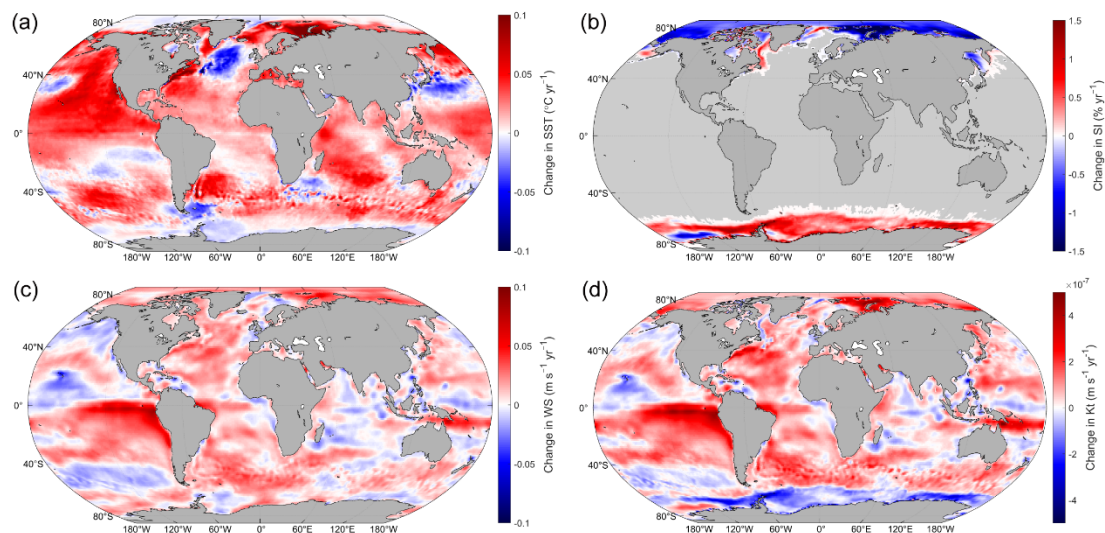
Figure S5. The spatial distributions of changes in (a) sea surface temperature (SST), (b) sea ice fraction (SI), and (c) surface wind speed (WS), and (d) DMS total transfer velocity (Kt) during 1998 to 2017.
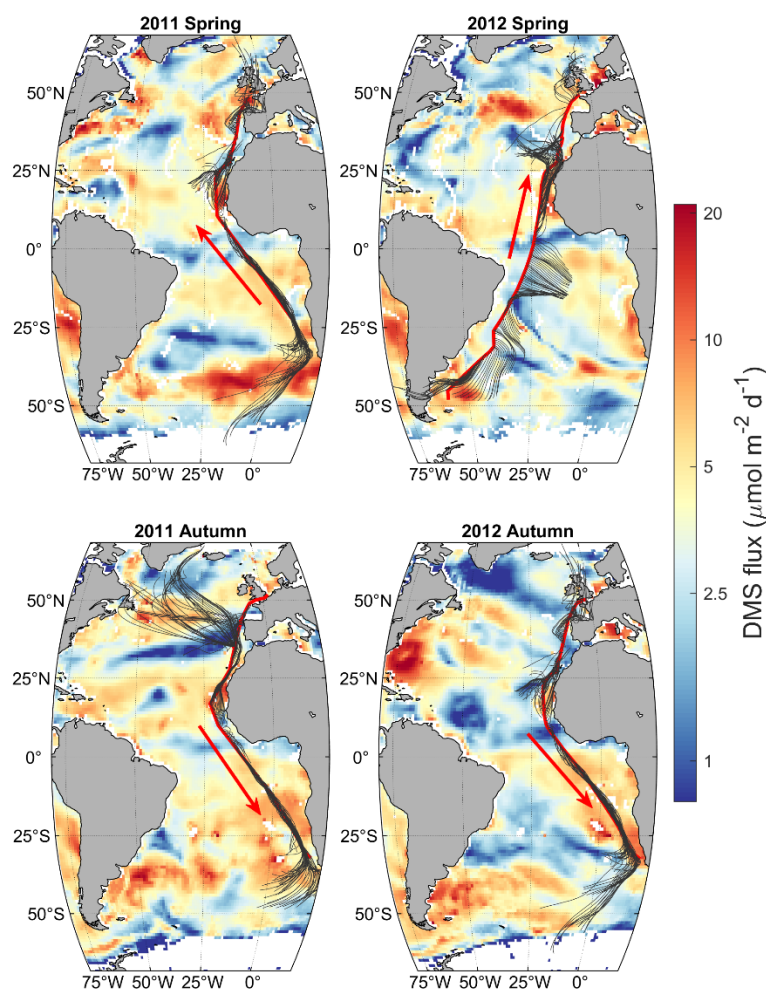
Figure S6. The ship tracks and 72-h air mass backward trajectories during four cruises in the Atlantic. The background is the average DMS flux during the time periods of each cruise based on Z23. The labelled seasons refer to seasons in the Northern Hemisphere.
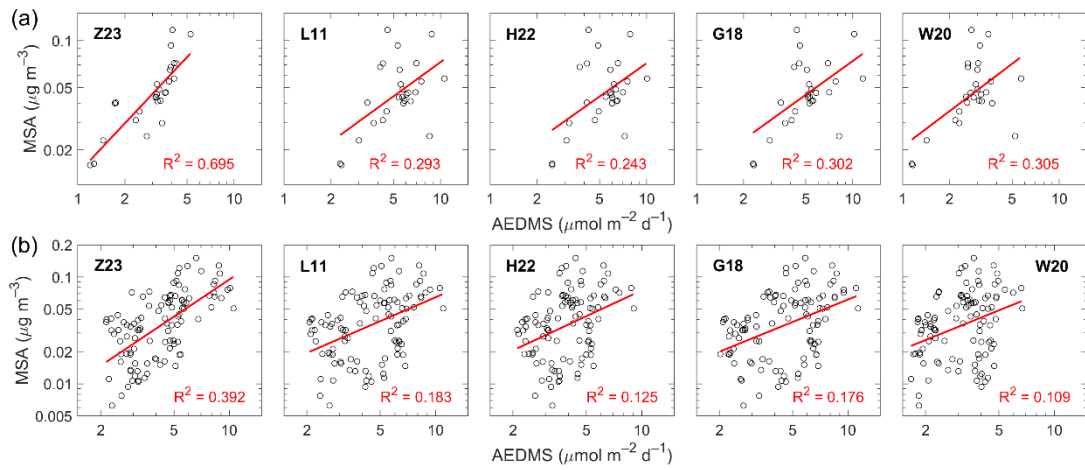
Figure S7. Correlations between 6-h averaged MSA concentration and AEDMS based on different DMS concentration datasets (a) in the region north of 25° N in boreal and (b) in the region south of 5° N in boreal autumn. Data points during the periods with airmass time fraction within boundary layer less than 90% were removed.